# Machine Learning Enhanced High Fidelity and High Viability Bioprinting using Rheological and Compositional Predictors



Proceedings of the IISE Annual Conference & Expo 2024 A. Brown Greer, C. Contardo, J.-M. Frayret, eds.

# Machine Learning Enhanced High Fidelity and High Viability Bioprinting using Rheological and Compositional Predictors

## Abstract ID: 7125

Authors: Mr. Imtiaz Qavi, Ms. Sampa Halder, Dr. Dongping Du and Dr. George Tan, Texas Tech University, Lubbock, TX

The field of 3D bioprinting is dynamically advancing, witnessing constant evolution through the introduction of novel materials, techniques, and strategies. A persistent challenge within this domain pertains to the optimization of materials and processes, aiming to achieve both a high cellular viability in the printed structure incorporating elisa and a faithful reproduction of the desired structure. The primary obstacle often encountered is the formulation of an appropriate bionik composition, exacerbated by the inherent variability in fluidic, rheological, and biocompatible characteristics. In this study, we investigated collagen-based bioniks crosslinked with alginates and reinforced with Laponite-RD nanoparticles. This formulation was explored as a potential yield-stress bioink, specifically addressing the dual challenge of ensuring high cellular viability and maintaining structural fidelity during bioprinting. Employing a Design of Experiment (DoE) methodology, we systematically gathered experimental data by varying material compositions. Subsequently, we assessed printability, extrudability, and the viscoelastic properties. The acquired data were utilized to train a hyperparameter-tuned machine learning (ML) model, enabling the prediction of inter-relationships among the responses. Furthermore, the ML model was instrumental in identifying the optimal compositional formulation. This formulation facilitated the fabrication of a high-fidelity structure with suitable extrudability, mitigating shear-induced cell death and ensuring high cell viability in the post-printed structure. In summary, our findings underscore the efficacy of a data-driven experimental design coupled with ML methodologies in shaping the future landscape of high-resolution and high-viability 3D bioprinting. This synergistic approach holds promise for overcoming existing challenges and advancing the frontier of precision in Bio-Fabrication. The field of 3D bioprinting is dynamically advancing, witnessing constant evolution through the introduction of

## Keywords

Machine Learning, Multi-Layer Perceptron, Neural Network, Biofabrication, Bioprinting, Rheology

## 1. Introduction

1. Introduction
Bioprinting, a dynamic field within biomedical engineering, enables the fabrication of sophisticated 3D structures for applications such as tissue/organ models, drug delivery modeling, and disease modeling. Current bioprinting technologies encompass inkjet, laser, extrusion, fused deposition modeling (FDM), stereolithography, and more [1], each with its own set of advantages and process-specific drawbacks. Among these, extrusion-based bioprinting stands out as the most widely used method for biofabrication, particularly for soft scaffold material structures in tissue engineering. It offers faster printing speed, a broader material selection, and low cytotoxicity [1]. A key challenge in bioink development is the viscoelastic nature of these materials, which is influenced by their complex rheological properties, such as storage modulus, shear-thining behavior, and viscosity recovery rate. These properties are crucial for ensuring that bioinks can be extruded from nozzles at relatively low pressures rate. These properties are crucial for ensuring that oftoms can be extruded from nozzies at reaturely presented for minimal cellular damage and successfully form continuous strands that maintain their predefined shapes upon deposition. Traditional methods for optimizing these properties typically rely on extensive experimental work, involving numerous trial-and-norro iterations. This approach can be both time-consuming and resource-intensive, making it a less efficient pathway to identifying optimal formulations. In addition, much of the existing research in this field tends to be material-specific, solely focusing on the material-printability relationship without understanding the rheological nature of the materials. The difficulty in generalizing results across materials highlights the mode for a more holistic approach to bioink research and the applicability of findings to the broader context of bioink development. development.

Addressing these challenges necessitates the development of models that correlate bioink rheological properties with print fidelity and extrusion pressures. This study employs a Multi-Layered Perceptron (MLP) based machine learning approach to construct predictive models that delineate the relationship between bioink rheology, printability, extrusion

pressure, and cellular viability. Employing data from a face-centered composite design of experiments for bioinks pressure, and centuar vaonity. Employing data from a face-centered composite design of experiments for holinst comprising laponite, sodium algiantet, and Type 1 collagen, we identified rheological attributes critical for optimizing print fidelity and minimizing extrusion pressure. In this bioink, laponite enhances structural integrity through its high storage modulus, algiantet ensures durability via cross-linking, and collagen promotes cell adhesion, providing essential biological cues. machine learning techniques in this optimization process of MLP models The integration of machine learning techniques demonstrate the efficacy of the MLP models in advancing bioink design for nextgeneration bioprinting applications with improved structural fidelity and cell viability.

#### 2. Materials and Methods

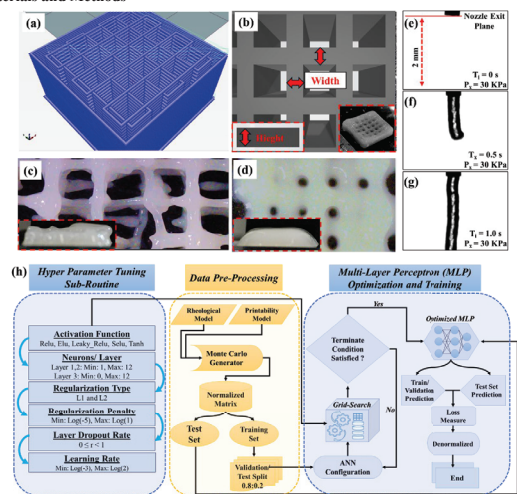


Figure 1: (a) 3D printing path for benchmarking printed structure conformity (PSC) (b) top view of 3D CAD grid model; bottom right inset shows typical printed grid structure (c) over-gelation bioprinting (d) under gelation bioprinting (e-g) filament growth at the minimum extrusion pressure (MEP) (h) Multi-layered Perceptron (MLP) model with grid-optimization hyper parameter tuning flow chart; Insets in b,c,d represent side views for height measurements.

#### 2.1. Bio-Ink ingredients and Bioprinting Process

Sodium Alginate (CAS 9005-38-3) was acquired from Sigma-Aldrich (MO, USA), Collagen from NeoCell Inc. (Irvine, CA), and Lapontie-RD from BYK (Wesel, Germany), Composites were generated by exploring a design space ranging from 0.1% to 2% for Collagen, 2% to 6% for Alginate, and 8% to 18% for Laponite (w/v %). Bioprinting was conducted using a Gauge G-20 needle with an internal diameter of 0.5 mm, facilitated by a custom-made 6-axis was controlled extrusion printer. A 3D grid shape (Figure 1a and 1b) with a total height of 5 mm was designed to evaluate

Printed Structure Conformity (PSC). PSC was assessed by comparing a printed structure in terms of the filament height and width with the original 3D grid model. The Minimum Extrusion Pressure (MEP) was determined as the pressure required for the composition to form a  $2\,\mathrm{mm}$ -long filament in 1 second, as illustrated in Figure 1e-f.

## 2.2. Rheological Parameters

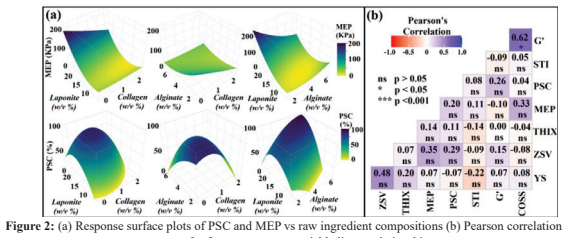
2.2. Authorogical rarameters
The rheological properties of the composite bio-inks were assessed using an Anton Paar MCR 92 Modular air-bearing rheometer (Austria) equipped with a 25 mm parallel plate rotor. Zero-shear viscosity (ZSV), yield stress (YS), and shear-thinning index (STI) were derived from the Carreau-Yasuda, Herschel-Bulkley, and Ostwald De Waele power shear-thinning index (S11) were derived from the Carreau-Yasuda, Herschel-Bulkley, and Ostwald De Waele power fit models, respectively [2]. Additionally, the cross-over shear stress (COSS) and storage modulus (G7) at the linear viscoelastic limit (LVER-G7) were determined through oscillatory sweep amplitude experiments, while the thixotropic viscosity recovery rate (THIX) was derived from variable shear-stress sweep modes. Incompatible and unoptimized rheological properties result in over and under-gelation of printed filaments that results in failed structures as depicted in Figure 1c and 1d.

2.3. Machine Learning Model and Optimization

The initial dataset of 20 data points, comprising the above mentioned six rheological parameters, Printed Structure Conformity (PSC), and Minimum Extrusion Pressure (MEP), was augmented using a Monte Carlo deterministic simulator with response-surface polynomial models. The synthetic data contains 1000 samples and were then split into training (75%) and testing (25%) data sets. The original 20 data points were reserved for the final model validation and the model training was performed fully on synthetic data for both training and testing. The training set was utilized to refine a 3-hidden layer Multi-Layered Perceptron (MLP) model through an optimal grid search method, while the testing set was used to evaluate the performance of the final MLP mode. The MLP optimization process encompassed determining the ideal activation functions (Arc Tan Tanh), rectified linear unit (ReLu), exponential linear unit (ELU), scaled exponential linear unit (SELU), and leaky rectified linear unit (Leaky\_ReLu)). Further optimization was scated exponential untar unit (SELU), and teaky rectified linear unit (Leaxy McLu), ruttner optimization was achieved by adjusting several parameters including the number of neurons per layer, the depart that for each layer, the L1/L2 regularization rates, and the learning rate for the model. The optimized models were learned using 80% of the training dataset and validated by 20% of the training dataset [3]. The machine learning procedures are illustrated in Figure 1G. This final model was then employed to construct a contour map illustrating the effects of rheological parameters (ZSV, STI, G', THIX, YS, COSS) on PSC and MEP. The insights gained from this map were pivotal to identify the optimal compositions of bioinks. The goal was to achieve a configuration where the MEP was minimized to less than 35 KPa while ensuring that the PSC remained above 80%.

# 3. Results and Discussion

# 3.1 Data visualization



map for feature-response variable linear relationship

The response surface plots of PSC and MEP are depicted in Figure 2a. Notably, when the concentrations of laponite exceeds 15 w/v %, the MEP values rise above 100 KPa, which is unsuitable for bioprinting. The optimal PSC (> 80% is achieved when the laponite is below 16  $\text{M}^{\circ}$  %, the collagen is around 1.5 w/v %, and the sodium alignate is approximately 4 w/v %. Pearson's correlation coefficient assesses the linear tendencies between different variables in a dataset [4]. A statistically significant Pearson's coefficient indicates strong or moderate linear correlations between two variables. As depicted in Figure 2b, no significant linear correlations are found between the rheological parameters and PCS or MEP, which indicates linear models may not be effective for capturing the underlying relationships Therefore, we investigate nonlinear models, such as a Multi-Layer Perceptron (MLP) neural network regression model, for this analysis.

#### 3.2 MLP Architecture and Performance

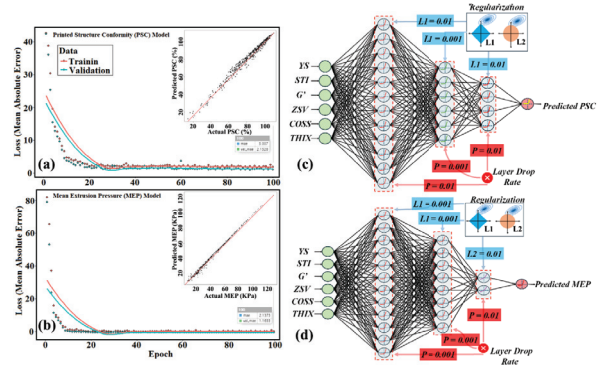


Figure 3: Validation and Training Loss (MAE) for the (a) PSC (b) MEP model. MLP architectures for the (c) PSC and (b) MEP model. Insets in (a) and (b) indicate the predicted vs actual PSC and MEP data using the optimized and trained models for the test data set (n = 250).

The evaluation of the model's performance is depicted through the loss metric, which is based on the mean absolute error (MAE). This metric is represented in the training and validation loss curves shown in Figure 3A and 3B. For both PSC and MEP, a notable reduction in loss was observed after 25 training epochs. The final validation loss for both datasets was as low as 5% of the original test data. Meanwhile the training and validation losses remained closely aligned throughout the training process. In typical machine learning scenarios, a significant gap between these two metrics can indicate overfitting, where the model performs well on the training data but poorly on new, unseen data. However, in this case, the training error rarely exceeded the validation error, suggesting that the models were well-calibrated and generalized effectively to new data. This consistent pattern across the training and validation phases demonstrates that the optimized models achieved a favorable balance in the bias-variance tradeoff.

The optimized and trained models, refined through grid-optimization techniques, are shown in Figure 3C and 3D. These schematics provide a comprehensive view of the architecture, including layer drop-rates, regularization values, and the number of neurons in each layer. The PSC model features a configuration of 12 ELU units in the first fidelen layer, followed by 6 SELU units in the second hidden layer, and 4 ELU units in the third hidden layer. The model

4

https://doi.org/10.21872/2024IISE\_7125

concludes with a ReLu activation function in the output neuron, a design choice that contributes to its effective performance. In contrast, the MEP model achieves its optimal performance in a different structure. It consists of 12 ELU units in the first hidden layer, 8 ELU units in the second hidden layer, and 2 Leaky ReLu units in the third hidden layer. The output neuron in this model employs an ELU activation function, a configuration that has proven effective for this specific application.

Furthermore, L1 regularization was applied to reduce overfitting and enhance model generalization. For the PSC model, L1 regularization values were set at 0.01, 0.001, and 0.01 to the three hidden layers, respectively. For the MEP model, the regularization values were set at 0.01 for the first and third layers, and 0.001 for the second layer. This strategic implementation of regularization plays a crucial role in the model's ability to accurately predict PSC while maintaining generalizability and robustness against overfitting. Notably, the final models showesed a high R-squared value of 0.95 and 0.98 in the actual vs. predicted plot when forecasting the original 20 data points reserved for final models where the product with the product of the p

## 3.2 Process Optimization

Desirability optimization was employed to determine the optimal configuration of feature variables that adhere to user-defined constraints on objective functions [5]. The maximization of the PSC objective function was conducted using a max-ramp with bounds set between 80% and 100%. Simultaneously, the MEP ramp was optimized using a min-ramp with bounds set between 10 and 35 KPa. The individual desirability indices are then combined to derive an overall desirability score, where D = 1 represents the maximum value [5]. To address varying priorities, the satisfaction criterion (w) was adjusted between 0, 1, and 2 for both the PSC and MEP ramps so that the models can achieve the optimal outcomes within the defined bounds.

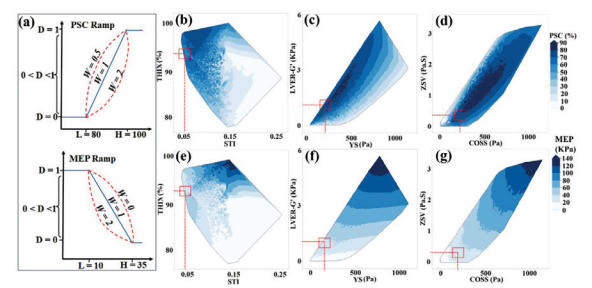


Figure 4: (a) Desirability ramps for the PSC (maximization) and MEP (minimization) model forms. Contour plots of different theological predictors and their corresponding response (b-d) PSC (b-g) MEP. The red highlighted box indicates optimality zones based on the desirability function optimization method.

Figures 4b-4d illustrate the contour maps of rheological properties plotted in the x-y planes, with color gradients representing the PSC values. The desirability ramps of MEP are shown in Figures 4e-g. Notably, an optimal solution is achieved when the thixotropic recovery rate exceed 94%, the shear-thinning index is 0.05, the yield stress stabilities around 100 Pa, the cross-over shear stress is 220 Pa, the LVER-G' reaches 1500 Pa, and the zero-shear viscosity maintains a minimum value of 0.4 Pa·s. This scenario yields an MEP value below 35 KPa and a PSC value over 90%. The optimal rheological values were then traced back to their initial laponite/alginate/gelatin concentrations using design-of-experiment-based response surface models.

Figure 5 shows the bioprinted high-fidelity structures, cellular viability, and porous microstructures resulting from Figure 5 snows the otoprinted night-inearity structures, ceilular viaonity, and porous microstructures resulting from the optimized bioinic composition (0.5% Collagen, 2.6 % Algiante, and 12.4% Laponite). Additional food coloring dye was added to the optimized bioink to facilitate easier observation and analysis. Remarkably, a single-layer print exhibited exceptional cellular viability, with over 95% viability (P > 0.001) for green fluorescence human umbilical vascular endothelial cells (GFP-HUVEC). The scanning electron microscope (GEM) micrographs revealed the presence of large porous structures within the bio-ink matrix which are critical for facilitating cellular proliferation and nutrient exchange

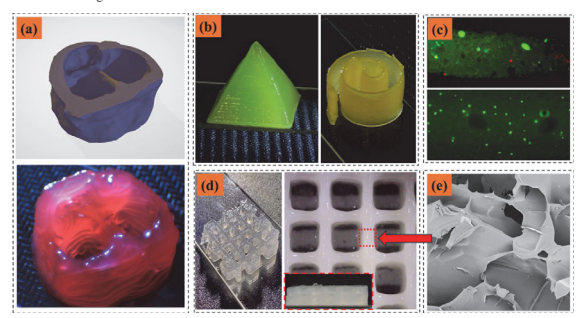


Figure 5: (a) 3D bio-printed human aortic valve (scale 1:0.7) (b) different printed shapes showing high-fidelity printing (c) cellular viability in single-layer prints at 33 KPa (d) top view high-fidelity grid structures; inset shows side view (e) Porous microstructures under SEM.

#### 4. Conclusion

4. Conclusion
This study introduces a machine learning based predictive approach for formulating bioinks with enhanced shape fidelity and cellular viability in 3D bioprinting applications. The objective was to optimize both structure conformity and extrusion pressures without compromising the post-printing cell viability. This work demonstrates the high efficacy of machine-learning-based non-linear regression techniques that can accurately forecast the printability of multi-material bioinks based on their compositions. While the current study models and optimizes printability structure conformity and minimum extrusion pressures, future investigations will extend to multiple response parameters, including mechanical properties, degradation, and long-term cell proliferation. In an industrial context, these machine-learning models can be integrated into advanced 3D printing systems with feedback loop control, allowing real-time adjustment to ensure material-independent and defect-free printing with high resolution.

#### References

- Benes Mobaraki, M., et al., Bioinks and bioprinting: A focused review. Bioprinting, 2020. 18: p. e00080.
  De Kee, D. and C. Chan Man Fong, Rheological properties of structured fluids. Polymer Engineering & Science, 1994. 34(5): p. 438-445.
  Géron, A., Hands-on machine learning with Scikit-Learn, Keras, and TensorFlow. 2022: "O'Reilly Media, Inc.".
  Sedgwick, P., Pearson's correlation coefficient. Bmj, 2012. 345.
  Costa, N.R., J. Lourenço, and Z.L. Pereira, Desirability function approach: a review and performance evaluation in adverse conditions. Chemometrics and Intelligent Laboratory Systems, 2011. 107(2): p. 234-244.

6

Reproduced with permission of copyright owner. Further reproduction prohibited without permission.